Fig. 1. Photographs of patient 1, age 5 years (a) and patient 2, age 4 years (b). Note that both patients have thin upper lips.

Table 1
Clinical features of *MAOA/B* deletion syndrome.

	Whibley et al.		Our patients		Total
	Patient 1	Patient 2	Patient 1	Patient 2	
IUGR (mild)	+	+	+	–	3/4
Short stature	+	+	+	+	4/4
Severe intellectual disability	+	+	+	+	4/4
Hypotonia	+	+	+	+	4/4
Sudden loss of muscle tone	+	+	+	+	4/4
Excitable behavior/self-injury	+	NA	+	+	3/3
Loss of sociability	NA	–	+	+	2/3
Sleep disturbance	NA	NA	+	–	1/2
Stereotypical hand movement	+	+	–	–	2/4
Lip smacking	+	+	+	+	4/4
Epicanthal fold	+	+	–	–	2/4
Long eyelashes	+	+	+	+	4/4
Thin upper lip	–	–	+	+	2/4
Cryptorchidism	–	–	+	+	2/4
Polydactyly	–	–	+	–	1/4

Bold were candidate for the feature of *MAOA/B* deletion syndrome.
IUGR, intrauterine growth retardation. NA, not available.

blind, at 3 months of age the patient exhibited repeated upward eye deviations for several seconds every day over the course of 1 month. At 4–18 months, he often experienced a sudden loss of muscle tone that induced falling down after laughter or excitement. Electroencephalogram (EEG) and cranial magnetic resonance imaging (MRI) were normal. At 12 months, the patient could sit on his own. Disturbed sleep patterns were observed around 13 months. Sometimes the patient repeatedly slept for half an hour at a time and screamed during awaking, often displaying abnormal and self-injurious behavior that included head banging, hand chewing, and scratching himself. At 3 years of age, the patient had not spoken any meaningful words, did not make eye contact, had little interest in other people, and was attached to spinning toys and shiny things. Therefore, the boy fulfilled the criteria of DSM-IV and was diagnosed with autism spectrum disorder (ASD). He did not exhibit stereotypic hand movements, but did show hand flapping and lip smacking. The sleep disturbances and abnormal behavior disappeared at 3 years of age when he began taking risperidone (0.2 mg/d). When he was 4 years old, the patient walked with support. At 5 years of age, he could walk several meters by himself and could say several meaningful words. At that time, his weight and height were 15.0 kg

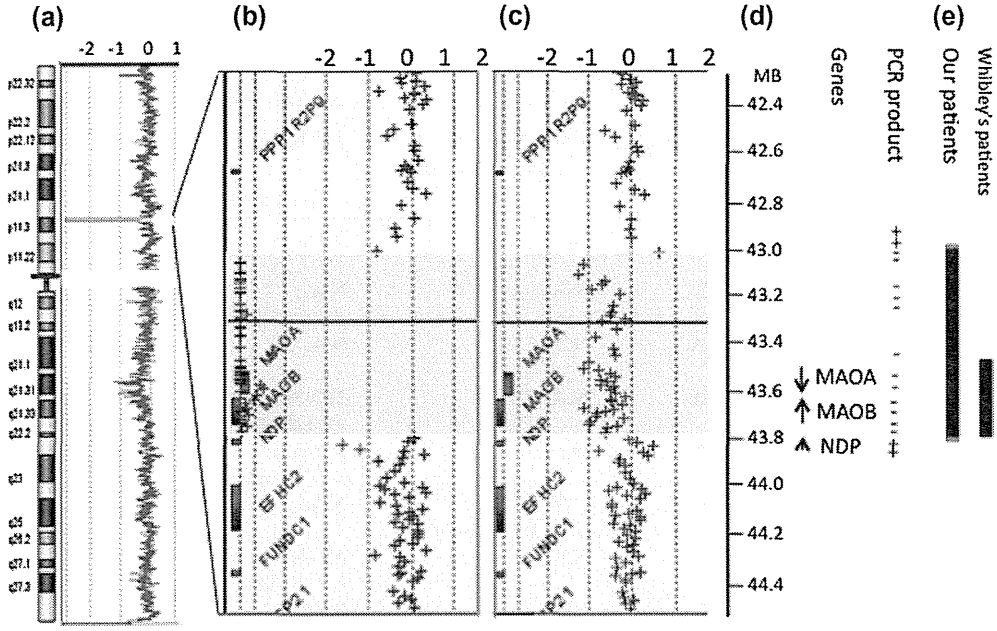

Fig. 2. Array-comparative genomic hybridization (aCGH) analysis and PCR confirmation of the deletion. (a) aCGH analysis of the entire X chromosome of patient 1. A deletion was detected on Xp11.3. (b) and (c) Detailed views of the microarray plots of patient 1 (b) and his mother (c). In the figure, + signals indicates the position of nucleotides on the array. The horizontal axis shows the fold-change in copy number variation. Note that "1" stands for "duplication of one chromosome", and "−1" stands for "deletion of one chromosome". The dark blue shaded area is the deleted region. Because there is just one X chromosome in males, the signal of the deletion in patient 1 was not detected, and + signals are located on the bottom. The mother showed heterozygous deletion. (d) The chromosomal position is indicated vertically as megabases from the centromere. The deletion size was confirmed by PCR as being approximately 800 kb (extending from about 43.0 MB to 43.8 MB). The deletion included just two genes, *MAOA* and *MAOB*. (e) A deletion was detected on Xp11.3 in patient 1. The schematic shows a comparison of the deletion in our two patients and in the patients reported by Whibley et al. [7].

(−1.3 SD) and 93.7 cm (−3.5 SD), respectively. At his medical examination, he had long eyelashes and a thin upper lip (Fig. 1a). An ophthalmological examination detected no abnormalities except for intermittent internal strabismus. He was hypotonic but had normal deep tendon reflexes (DTR).

Patient 2 was a 4-year-old boy who was the younger brother of patient 1. He was born at 38 weeks of gestation with a birth weight of 2750 g, which was normal for his gestational age. This patient also had bilateral cryptorchidism and was not blind. Around 7 months of age, he often lost muscle tone suddenly after laughing or taking a bath. At 1 year, he could sit unassisted. At 2 years of age, the boy demonstrated some eye gaze but did not use verbal or non-verbal methods to express requests. The patient was diagnosed with pervasive developmental disorder not otherwise specified according to the criteria of the DSM-IV. He demonstrated self-injurious and lip-smacking behaviors, but did not show sleep disturbances or stereotypic hand movements. Risperidone (0.2 mg/d) was started at age 3 years. When he was 4 years old, the patient's weight and height were 13.2 kg (−1.0 SD) and 87.7 cm (−2.9 SD), respectively. He could stand with support, and he spoke some meaningful words. At his medical examination, he had long eyelashes and a thin upper lip (Fig. 1b). Findings from his ophthalmological examination were normal except for intermittent strabismus. His EEG and cranial MRI results were unremarkable. The clinical features of the patients are listed in Table 1.

Consent for publishing their photographs was obtained from their patients.

2.2. Array CGH analysis

Genomic DNA was isolated from the lymphocytes of the two boys and their mother after obtaining informed consent of their parents. We performed array-comparative genomic hybridization (aCGH) following the manufacturer's protocol using the Human Genome CGH microarray 180 K (Agilent Technologies, Santa Clara, CA, USA). Male and female genomic DNA (Promega, Madison) were used as references in the sex-match hybridizations, and the aCGH results were analyzed with CGH-analytics software v3.4.

2.3. PCR confirmation of the deletion size

Two exons of *MAOA* (exons 4 and 7) and two exons of *MAOB* (exons 3 and 6), plus STS markers or arbitrary selected sequences in and around the deleted

Table 2
Monoamine profiles in urine, cerebral spinal fluid (CSF), and serum in the patients in this study and in patients with atypical Norrie disease, MAOA deletion and MAOB deletion.

	This study		Collins, et al.[5]	Brunner, et al.[2]	Lenders, et al.[3]
	Patient 1	Patient 2	1 patient	3 patients	5 patients
			Atypical Norrie dis.		
(Urine)	MAOA, MAOB deletion			MAOA deletion	MAOB deletion
Dopamine	**1.88** 0.07 ± 0.22 mg/g Cr	**1.45**	**N.A.***	**N.A.**	**905–2666** 516 ± 162 nmol/mmol Cr
Norepinephrine	**0.29** 0.27 ± 0.19 mg/g Cr	**2.6**	**N.A.**	**N.A.**	**106–461** 180 ± 127 nmol/mmol Cr
Epinephrine	**N.A.**	**N.A.**	**N.A.**	**N.A.**	**189** <3.01 nmol/mmol Cr
3-MT	**N.A.**	**N.A.**	**N.A.**	**217–318** 37–118 nmol/mmol Cr	**947–2910** 40 ± 10 nmol/mmol Cr
Normetanephrine	**4.7** 0.39 ± 0.12 mg/g Cr	**3.27**	**N.A.**	**392–666** 34–182 nmol/mmol Cr	**1524–2908** 240 ± 74 nmol/mmol Cr
Metanephrine	**0.47** 0.11 ± 0.06 mg/g Cr	**0.27**	**2.98** 0.39 ± 0.12 mg/g Cr	**N.A.**	**162–247** 63 ± 34 nmol/mmol Cr
MHPG	**N.A.**	**N.A.**	**N.A.**	**0.1–0.2** 0.1–2.1 μmol/mmol Cr	**55–111** 805 ± 129 nmol/mmol Cr
HVA	**1.18** 5.74 ± 2.32 mg/g Cr	**<0.1**	**0.58**	**0.4–0.5** 1.0–5.0 μmol/mmol Cr	**360–5103** 3564 ± 1440 nmol/mmolCr
VMA	**<0.1** 3.24 ± 0.91 mg/g Cr	**<0.1**	**0.39**	**0.2–0.4** 0.5–7.6 μmol/mmol Cr	**~508** 1849 ± 519 nmol/mmol Cr
Serotonin	**N.A.**	**N.A.**	**N.A.**	**124–233** 11-68 nmol/mmol Cr	**256** 10–78 nmol/mmol Cr
5-HIAA	**N.A.**	**N.A.**	**N.A.**	**0.8–1.4** 0.3–5.1 μmol/mmol Cr	**N.A.** 10–40 nmol/mmol Cr
(*CSF*)					
Dopamine	**17** 10–50 pg/mL	**18**	**N.A.**		
Norepinephrine	**409** 180 ± 17 pg/mL	**286**	**365**		
HVA	**N.A.**	**N.A.**	**8.9** 32.3 ± 2.4 ng/mL		
Serotonin	**3000** <10 pg/mL	**2800**	**1740**		
5-HIAA	**<1.0** 24.6 ± 1.8 ng/mL	**<1.0**	**0.22**		
(*Serum*)					
Dopamine	**18** <20 pg/mL	**18**			
Norepinephrine	**358** 100–450 pg/mL	**864**			
Serotonin	**0.06** 0.04-0.35 μg/mL	**1.74**			
5-HIAA	**<1.0** 1.8–6.1 ng/mL	**<1.0**			

Reference values were noted under the patient values. *N.A. = Not available.
3-MT, 3-methoxythramine; MHPG, methoxyhydroxyphenylglycol; HVA, homovanillic acid; VMA, vanillylmandelic acid; 5-HIAA, 5-Hydroxyindoleacetic acid.

region, were amplified by PCR from genomic DNA from each patient and from control subjects. The PCR reaction was performed using the GeneAmp PCR system 9700 (Applied Biosystems, Carlsbad, CA, USA) with 5 min denaturation at 94 °C, followed by 30 cycles of 94 °C for 30s , 30 s at the annealing temperature of each primer, and 30 s at 72 °C. The PCR products were evaluated by electrophoresis on 1% agarose gels stained with ethidium bromide.

This study was approved by the Bioethics Committee for Human Gene Analysis at Jichi Medical University,

3. Results

3.1. aCGH analysis

aCGH analysis of the two boys showed a deletion on Xp11.3 in the region where *MAOA* and *MAOB* are

located (Fig. 2a and b; only patient 1 is shown). PCR amplification revealed that both MAO genes, but not *NDP*, were deleted in both patients. The deletion size was approximately 800 kb and extended from about 43.0 MB to 43.8 MB. The only genes in the deletion were the *MAOA* and *MAOB* (Fig. 2d). Therefore, the karyotype of the two boys was 46, XY, del(X)(q11.3q11.3). The unaffected mother of the patients showed heterozygous deletion in that region (Fig. 2c).

3.2. Serotonin and catecholamine levels in the CSF and serum

The serotonin and catecholamine levels in the urine, CSF, and serum are listed in Table 2. The CSF 5-HT level was significantly elevated in patients 1 and 2 to 3000 and 2800 pg/ml (control, <10), respectively. The serum serotonin level was normal in patient 1 as 0.06 μg/ml, but was elevated to 1.74 μg/ml (control, 0.04–0.35) in patient 2. 5-hydroxyindoleacetic acid (5-HIAA), a metabolite of serotonin, was undetectable in the CSF and serum of both patients, i.e. ⩽1.0 ng/ml (control, 24.6 ± 1.8). The CSF norepinephrine (NE) level was mildly elevated to 409 and 286 pg/ml (control, 180 ± 17) in patients 1 and 2, respectively, and the CSF dopamine levels were 17 and 18 pg/ml (control, 10–50), respectively, which is in the normal range. The serum NE levels were 358 and 864 pg/ml (control, 110–450) and the serum dopamine levels were 18 and 18 pg/ml (control, <20), in patients 1 and 2, respectively.

4. Discussion

MAOA/B deletion syndrome should be recognized as a distinct disorder that affects these patients and that affects the siblings reported previously as having the *MAOA/B* deletion [7]. The features of *MAOA/B* deletion syndrome include short stature, hypotonia, severe ID, episodes of sudden muscle tone loss, excitation, stereotypic hand movements, lip-smacking, and long eyelashes (Table 1). ASD may be one of the clinical features associated with this syndrome. Sudden muscle tone loss was a conspicuous feature. The patients suddenly lost muscle tone and dropped to the ground in a state that appeared to be similar to cataplexy of narcolepsy [7,8]. The mechanism underlying this might be related to abnormal catecholaminergic and cholinergic activities that were also considered for cataplexy. Further, the possibility of sudden low blood pressure or reduced heart rate should be investigated because an increased baroreceptor response and consequent hypotension or heart rate reduction has been detected in *Maoa/b*-deficient mice [9]. Loss of MAO resulted in extremely high serotonin levels and mild elevation of NE in the CSF (Table 2). Urinary and serum catecholamine and serotonin levels were also elevated, but their levels were variable (Table 2). The severe ID and abnormal behavior seen in these *MAOA/B*-deletion patients might be the result of high serotonin levels in the CNS. A number of studies have reported about serotonin toxicity for CNS. MAO inhibitor overdose induces high levels of serotonin, resulting in a serotonin syndrome that is characterized by confusion and excitation. CNS signs are commonly seen after birth in infants exposed to selective serotonin reuptake inhibitors in utero [10]. Risperidone, a serotonin receptor type 2 and dopamine receptor type 2 antagonist, diminished self-injurious behavior and insomnia in these patients and improved their social impairment, although the effect was not conclusive.

Several reported patients with *MAOA/B* deletion including atypical Norrie disease have died unexpectedly [7]. Identification and characterization of additional *MAOA/B* deletion patients and in-depth analysis of the features of this syndrome, including sudden death, is required.

Acknowledgement

This work was supported in part by research grants from the Kawano Masanori Memorial Foundation for the Promotion of Pediatrics and from the Ministries of Education, Science and Culture, Japan.

References

[1] Shih JC, Chen K, Ridd MJ. Monoamine oxidase: from genes to behavior. Ann Rev Neurosci 1999;22:197–217.
[2] Brunner HG, Nelen M, Breakefield XO, Ropers HH, van Oost BA. Abnormal behavior associated with a point mutation in the structural gene for monoamine oxidase A. Science 1993;262:578–80.
[3] Lenders JW, Eisenhofer G, Abeling NG, Berger W, Murphy DL, Konings CH, et al. Specific genetic deficiencies of the A and B isoenzymes of monoamine oxidase are characterized by distinct neurochemical and clinical phenotypes. J Clin Invest 1996;97:1010–9.
[4] Murphy DL, Sims KB, Karoum F, de la Chapelle A, Norio R, Sankila EM, et al. Marked amine and amine metabolite changes in Norrie disease patients with an X-chromosomal deletion affecting monoamine oxidase. J Neurochem 1990;54:242–7.
[5] Collins FA, Murphy DL, Reiss AL, Sims KB, Lewis JG, Freund L, et al. Clinical, biochemical, and neuropsychiatric evaluation of a patient with a contiguous gene syndrome due to a microdeletion Xp11.3 including the Norrie disease locus and monoamine oxidase (MAOA and MAOB) genes. Am J Med Genet 1992;42:127–34.
[6] Suarez-Merino B, Bye J, McDowall J, Ross M, Craig IW. Sequence analysis and transcript identification within 1.5 MB of DNA deleted together with the NDP and MAO genes in atypical Norrie disease patients presenting with a profound phenotype. Hum Mut 2001;17:523.
[7] Whibley A, Urquhart J, Dore J, Willatt L, Parkin G, Gaunt L, et al. Deletion of MAOA and MAOB in a male patient causes

severe developmental delay, intermittent hypotonia and stereotypical hand movements. Eur J Hum Genet 2010;18:1095–9.
[8] Vossler DG, Wyler AR, Wilkus RJ, Gardner-Walker G, Vlcek BW. Cataplexy and monoamine oxidase deficiency in Norrie disease. Neurology 1996;46:1258–61.
[9] Holschneider DP, Scremin OU, Roos KP, Chialvo DR, Chen K, Shih JC. Increased baroreceptor response in mice deficient in monoamine oxidase A and B. Am J Physiol Heart Circ Physiol 2002;282:H964–72.
[10] Moses-Kolko EL, Bogen D, Perel J, Bregar A, Uhl K, Levin B, et al. Neonatal signs after late in utero exposure to serotonin reuptake inhibitors: literature review and implications for clinical applications. JAMA 2005;293:2372–83.

LIN7A Depletion Disrupts Cerebral Cortex Development, Contributing to Intellectual Disability in 12q21-Deletion Syndrome

Ayumi Matsumoto[1☯], Makoto Mizuno[2☯], Nanako Hamada[2], Yasuyuki Nozaki[1], Eriko F. Jimbo[1], Mariko Y. Momoi[1], Koh-ichi Nagata[2], Takanori Yamagata[1]*

1 Department of Pediatrics, Jichi Medical University, Tochigi, Japan, **2** Department of Molecular Neurobiology, Institute for Developmental Research, Aichi Human Service Center, Kasugai, Japan

Abstract

Interstitial deletion of 12q21 has been reported in four cases, which share several common clinical features, including intellectual disability (ID), low-set ears, and minor cardiac abnormalities. Comparative genomic hybridization (CGH) analysis using the Agilent Human Genome CGH 180K array was performed with the genomic DNA from a two-year-old Japanese boy with these symptoms, as well as hypoplasia of the corpus callosum. Consequently, a 14 Mb deletion at 12q21.2-q21.33 (nt. 77 203 574–91 264 613 bp), which includes 72 genes, was detected. Of these, we focused on *LIN7A*, which encodes a scaffold protein that is important for synaptic function, as a possible responsible gene for ID, and we analyzed its role in cerebral cortex development. Western blotting analyses revealed that Lin-7A is expressed on embryonic day (E) 13.5, and gradually increases in the mouse brain during the embryonic stage. Biochemical fractionation resulted in the enrichment of Lin-7A in the presynaptic fraction. Suppression of Lin-7A expression by RNAi, using *in utero* electroporation on E14.5, delayed neuronal migration on postnatal day (P) 2, and Lin-7A-deficient neurons remained in the lower zone of the cortical plate and the intermediate zone. In addition, when Lin-7A was silenced in cortical neurons in one hemisphere, axonal growth in the contralateral hemisphere was delayed; development of these neurons was disrupted such that one half did not extend into the contralateral hemisphere after leaving the corpus callosum. Taken together, *LIN7A* is a candidate gene responsible for 12q21-deletion syndrome, and abnormal neuronal migration and interhemispheric axon development may contribute to ID and corpus callosum hypoplasia, respectively.

Citation: Matsumoto A, Mizuno M, Hamada N, Nozaki Y, Jimbo EF, et al. (2014) LIN7A Depletion Disrupts Cerebral Cortex Development, Contributing to Intellectual Disability in 12q21-Deletion Syndrome. PLoS ONE 9(3): e92695. doi:10.1371/journal.pone.0092695

Editor: Barbara Bardoni, CNRS UMR7275, France

Received November 19, 2013; **Accepted** February 24, 2014; **Published** March 21, 2014

Funding: This work was supported by the grant from Ministry of Education, Culture, Sports, Science and Technology of Japan (grant number 23390275), MEXT-Supported Program for the Strategic Research Foundation at Private Universities 2011–2015 (Cooperative Basic and Clinical Research on Circadian Medicine). And also Grants-in-Aid for Scientific Research on Priority Area, Challenging Exploratory Research and Scientific Research (B) from the Ministry of Education, Culture, Sports, Science and Technology, Japan and a grant from Takeda Science Foundation. The funders had no role in study design, data collection and analysis, decision to publish, or preparation of the manuscript.

Competing Interests: The authors have declared that no competing interests exist.

* E-mail: takanori@jichi.ac.jp

☯ These authors contributed equally to this work.

Introduction

Interstitial deletion of 12q21 has been reported in four cases since 1999 [1–4]. Common clinical features of this deletion include: intellectual disability (ID), low-set ears, sparse hair, prominent forehead, hyper- or hypo-telorism, minor cardiac abnormalities, and cutaneous findings, such as hyperkeratotic papular eruption and atopic dermatitis. These phenotypes resemble those in cardiofaciocutaneous (CFC) syndrome, which is characterized by a distinctive facial appearance, heart defects, and ID [5]. However, while genes on the RAS-MAPK pathway have been identified as the causative genes for CFC syndrome, no genes related to this signaling pathway are located within the reported deleted regions of 12q21.

Outside of the RAS-MAPK pathway, many genes that are related to synaptic function and plasticity have been reported as responsible for ID [6,7]. Lin7 – the product of the *LIN7* gene – is known to play a crucial role in synapse functions. Lin7 is a small scaffold protein containing a L27 and a PDZ domain at the N- and C-terminus, respectively. The L27 domain mediates hetero-dimerization with several membrane-associated guanylate kinase (MAGUK) proteins – including calcium/calmodulin-dependent serine protein kinase (CASK), protein associated with LIN-7 (Pals), synapse-associated protein 97 (SAP97), and PSD95/93 – which form the core of the protein complexes that mediate synaptic development, plasticity, and functionality [8]. On the other hand, the PDZ domain (corresponding to the first letters of PSD-95, Discs-large, and ZO-1) binds with many proteins, which are essential for neuronal cell polarity, cell adhesion, and cell signaling [9].

Accumulating evidence has uncovered a possible relationship of *LIN7* with neuronal disorders. Vertebrates have three *LIN7* isoforms, *LIN7A–C*, also known as *MALS/Veli1–3* [10,11]. Recently, polymorphisms of *LIN7* have also been shown to be associated with attention-deficit/hyperactivity disorder (ADHD) [12], and microdeletions at 11p14.1 (where *LIN7C* is localized) are

reportedly associated with ADHD, autism, and developmental delay [13]. Furthermore, decreased Lin-7B expression in pyramidal neurons in cerebral cortex layer V may contribute to impaired neuronal connectivity in Huntington's disease [14].

The present study describes a Japanese boy who presented facial dysmorphism and ID, similar to previously reported patients with 12q21 deletion. Using array comparative genomic hybridization (CGH) analysis, we identified a deletion at 12q21.2–q21.33, which is the narrowest deletion found in a patient with 12q21-deletion syndrome to date. Among the genes located in the deleted region, we focused on *LIN7A*, performing biochemical and RNAi analyses to clarify the pathophysiological significance of Lin-7A in 12q21-deletion syndrome. While Lin-7A did not appear to be involved in neuronal cell proliferation, we determined that loss of Lin-7A function induced defective migration and axonal growth of excitatory pyramidal neurons during corticogenesis. Thus, functional defects of Lin-7A are likely to cause defective cortical development, leading to ID in 12q21-deletion syndrome.

Materials and Methods

Ethics statement

This study was approved by the bioethics committee for human gene analysis at Jichi Medical University (approval number: 11–14). Written informed consent was obtained from the mother for the child and herself, and from the father for himself. We followed the Fundamental Guidelines for Proper Conduct of Animal Experiment and Related Activities in Academic Research Institutions under the jurisdiction of the Ministry of Education, Culture, Sports, Science and Technology, and all of the protocols for animal handling and treatment were reviewed and approved by the Animal Care and Use Committee of Institute for Developmental Research, Aichi Human Service Center (approval number, M10).

Patient report

The patient was a boy of two years and 11 months of age. He was the first child born to a non-consanguineous and healthy 24-year-old mother and 26-year-old father. The patient was born by cesarean section at 38 weeks and three days. At birth, his height, weight, and occipito-frontal circumference were 45.6 cm (1.64 SD), 2330 g (1.40 SD), and 32.3 cm (0.60 SD), respectively. His growth parameters were normal.

At two years and 11 months of age, the boy's developmental quotient (DQ) was 20, according to the kinder infant development scale (KIDS). He could sit without support but could not walk or speak any meaningful words. He showed prominent forehead, hypotelorism, short upturned nose, long philtrum, small mandible, high-arched palate, low-set ears, sparse hair, and internal strabismus. He also had mild spastic diplegia, and his neurological evaluation revealed hyperreflexia of the patellar and Achilles tendon reflexes. Cranial magnetic resonance imaging (MRI) showed ventriculomegaly and mild hypoplasia of the corpus callosum (Figure 1).

Array CGH analysis

After obtaining blood from the patient and his parents, lymphocytes were extracted, and lymphoblasts were established by Epstein–Barr virus. Array CGH analysis was performed using the Agilent Human genome CGH 180K (Agilent Technologies, Santa Clara, CA, USA). In brief, DNA was isolated from the lymphocytes, using the DNeasy Blood and Tissue kit (Qiagen, Hilden, Germany), according to the manufacturer's instructions. Genomic DNA (1 μg) from the patient and reference DNA

Figure 1. Cranial MRI findings at 10 months of age. Sagittal and T1-weighted image, showing mild hypoplasia in the corpus callosum.
doi:10.1371/journal.pone.0092695.g001

samples from unaffected volunteers (Coriell Institute for Medical Research, Camden, New Jersey, USA) were labeled with fluorescent dyes (Cy5-dUTP and Cy3), hybridized at 65 °C for 24 hours, and then subjected to the array. The hybridized array was scanned with an Agilent DNA Microarray Scanner (Agilent Technologies). The resulting images were analyzed by quantifying the Cy3 and Cy5 fluorescence intensity at each feature on the array, using the Agilent Feature Extraction Software (Agilent Technologies). Finally, the data were calculated using the Agilent Workbench Software (Agilent Technologies).

Plasmids

Human LIN7B-encoding cDNA was obtained as previously described [15]. Mouse Lin7A, Lin7B, and human Lin7A were obtained by PCR from brain cDNA pools, and ligated into pCAG-Flag, pCAG-Myc, or pCAG-GFP vectors. All constructs were verified by DNA sequencing.

RNA interference

Modifications of the pSUPER-puro vector (OligoEngine, Seattle, WA, USA) were designed to target two distinct coding sequences in m*Lin7A*: pSUPER-mLin7A#1 targets 5′-GTGTATCAATACATGCATG-3′, 202–220; and pSUPER-mLin7A#2 targets 5′-GTTGAACTGCCAAAGACTG-3′, 325–343 (numbers indicate the position from the transcription start site). As an RNAi-resistant version of mLin7A, we used the human ortholog hLin7, in which the target sequence against pSUPER-mLin7A#1 contains a mismatched nucleotide (5′-GTGTATCAATATATGCATG-3′) as marked with an underline. The target sequences for pSuper-mLin7A#1 and #2 contain mismatched nucleotides when compared to the corresponding sequences in mLin7B (targets 5′-GTGTATGAACAGCTCTATG-3′, 5′-GTGGAACTACCGAAGACTG-3′), respectively, as marked with underlines.

Cell culture and transfection

COS cells were cultured essentially as previously described [16]. Transient transfection was carried out using the Lipofectamine method (Invitrogen, Carlsbad, CA, USA).

Primary antibodies

We generated polyclonal rabbit anti-Lin7 antibodies against affinity-purified bacterially synthesized human Lin-7B [15]. Characterization of anti-Lin7 was performed previously [15]. Polyclonal rabbit anti-GFP was prepared as described [17]. The mouse monoclonal antibody against glial fibrillary acidic protein (GFAP) was purchased from Chemicon (Temecula, CA, USA). Mouse monoclonal anti-β-tubulin, anti-Flag M2, and rabbit polyclonal anti-Flag were purchased from Sigma (Tokyo, Japan).

Subcellular fractionation of rat brain

Subcellular fractionation of fresh adult rat brains was performed essentially as described previously [18].

In utero electroporation

Pregnant ICR mice were purchased from SLC Japan (Shizuoka, Japan). *In utero* electroporation was performed essentially as described previously [19,20]. Briefly, 2 μL of nucleotide solution containing expression plasmids and pSUPER-RNAi plasmid (2 μg each) was introduced into the lateral ventricles of embryos, followed by electroporation using a CUY21 electroporator (NEPA Gene, Chiba, Japan) with 50 ms of 30 V electronic pulses, six times with 950 ms intervals. It is most likely that the expression and RNAi plasmids were efficiently co-transfected into the majority of the neuronal progenitor/stem cells at the transfected region [19]. All electroporations were performed on embryonic day 14.5 (E14.5), and at least five brains were used for each experiment.

Quantitative estimation of neuronal migration

The distribution of GFP-positive cells in brain slices was quantified, as follows: Coronal sections of cerebral cortices containing the labeled cells were classified into four regions: layers II–IV and V–VI, and the IZ and SVZ/VZ, as described previously [21]. The number of labeled cells (>100) in each region was calculated for least three slices per brain.

EdU incorporation experiment

Embryos were electroporated *in utero* at E14 with the pCAG-EGFP vector and the pSUPER vector (control) or pSUPER-mLin7A#1. Thirty hours after electroporation, pregnant mice were given an intraperitoneal injection of EdU (25 mg/kg body weight). One hour after the injection, embryonic brains were fixed with 4% paraformaldehyde, and vibratome sections were made. Finally, GFP and EdU were detected with anti-GFP and Alexa Fluor555 azide (Life Technologies, Palo Alto, CA, USA), following the manufacturer's protocol.

Statistical analysis

Results are expressed as mean ± s.e.m. When data were obtained from only two groups, Student's *t*-test was used for comparison. The rate of cell scores were initially analyzed using the one-way analysis of variance (ANOVA). Subsequently, a Fisher's least-significant difference (LSD) test was applied to absolute values as a *post-hoc* test of multiple comparisons. A P value of <0.05 was considered to indicate statistical significance. Statistical analysis was performed using Statview software (SAS Institute, Cary, NC, USA).

Results

Chromosomal analysis

The karyotype of the proband's amniotic cells was 46, XY, inv(12)(q12.q21). His mother's karyotype was 46, XX. His father had a karyotype of mos 46, XY/46, XY, inv(12)(q12q21) of 74:6 cells in lymphocytes, without phenotype. A highly accurate analysis of chromosome 12 in lymphocytes detected an inversion of 12q13.1–q21.2 and a deletion at 12q21.2–q21.3 (Figure S1).

Array CGH analysis

In the proband, CGH analysis using the Agilent Human genome CGH 180K array detected a 14 Mb deletion at 12q21.2–q21.33 (nt. 77 203 574–91 264 613) (Figure 2B). Therefore, the patient's karyotype was confirmed as 46, XY, del(12)(q21.2-q21.33)inv(12)(q13.1q21.2). Array CGH analysis of his parents did not detect this 12q21 deletion (Figure 2B).

The gene encoding the zinc finger DHHC domain containing protein 17 *(ZDHHC17)* was disrupted at the break point of the deleted region at 77.2 Mb; a gene does not exist at the other break point at 91.3 Mb. Among the 72 genes located in this deleted region, several appeared as potentially important in relation to neuronal development and function, including *ZDHHC17*, neuron navigator 3 *(NAV3)*, synaptotagmin 1 *(SYT1)*, PRKC apoptosis WT1 regulator *(PAWR)*, *LIN7A*, etc. (Figure 2C). Here we focused on *LIN7A* as a candidate gene for ID and hypoplasia of the corpus callosum in this syndrome, and investigated its pathophysiological relevance.

Developmentally regulated Lin-7 expression in the rat brain

Although abnormal corticogenesis and synapse formation may contribute to the emergence of ID [22], Lin-7 expression has only been analyzed fragmentarily in the cerebral cortex during the developmental stage. Therefore, Lin-7 protein expression during embryonic and postnatal brain development was determined by western blot analysis. Lin-7A and Lin-7B/C were detected in the cerebral cortex from E13.5 to P30 with characteristic expression profiles (Figure 3A, upper panel). Lin-7A was first detected at E13.5, gradually increased during the embryonic stage, and then dramatically increased after P15, while the Lin-7B/C level increased gradually throughout the analyzed developmental stage. The developmental process was confirmed by visualizing the glial cell differentiation marker GFAP (Figure 3A, lower panel). These results suggest different roles of the Lin-7 isoforms during neuronal development.

Immunohistochemical staining and *in situ* hybridization further revealed that Lin-7A–C are differentially expressed in discrete populations of neurons throughout the adult mouse brain. Most neurons express only one Lin-7 isoform, although some cells contain two or even all three isoforms [23]. We then examined the subcellular fractionation of the cerebral cortex, and found that Lin-7A was comparably enriched in the presynaptic membranes, while Lin-7B/C tended to be present with a postsynaptic density (PSD) fraction (Figure 3B). Immunohistochemical analyses supported these findings, as Lin-7 was visualized in axons/dendrites of neurons in the thalamus, hippocampus CA1 region, and dentate gyrus in the adult rat brain [15]. These results indicate a possibility that Lin-7 isoforms have spatiotemporally specific roles during brain development and in synapse formation, maintenance, and functions.

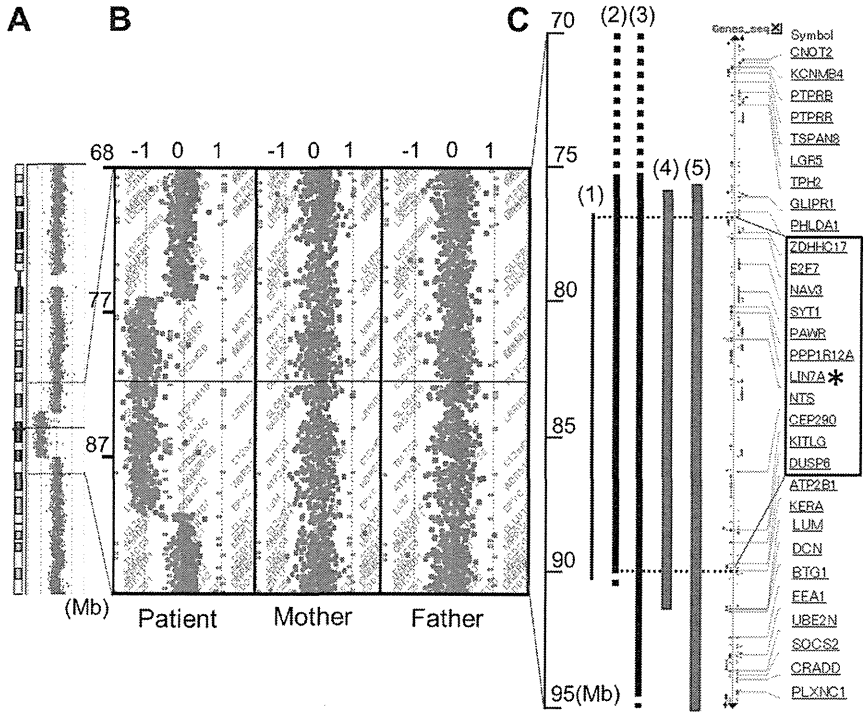

Figure 2. Array CGH analysis of chromosome 12. (**A**), Array CGH analysis of the entire chromosome 12 in the patient, showing a 14-Mb deletion of 12q21.2–q21.33 (77.2–91.2 M). (**B**), Detailed views of the microarray plots for the patient and his parents. The vertical axis shows megabases (Mb) from the telomere of 12q, and the horizontal axis shows the fold-change in copy number variation. (**C**), Comparison of the deleted positions. Bars indicate the deletion of the patient. (1) our patient, (2) Rauen, et al., 2002, (3) Klein, et al., (4) Brady, et al., and (5) Rauen, et al., 2000, respectively. The main genes existing in this area were listed as modified NCBI data. Genes surrounding *LIN7A*, from *ZDHHC17* to *DUSP6*, which are enclosed by the square, were included in the common deleted region from all five cases. An asterisk indicates *LIN7A*.
doi:10.1371/journal.pone.0092695.g002

Role of Lin-7A in neuronal migration during corticogenesis

To investigate whether *LIN7A* deletion may induce abnormal cerebral cortex cytoarchitecture leading to ID, we performed RNAi experiments, and examined the role of Lin-7A in the migration of newly generated cortical neurons during brain development. We designed two RNAi vectors – pSUPER–mLin7A#1 and pSUPER–mLin7A#2 – against distinct regions in the *mLin-7A* coding sequence. Both vectors efficiently knocked down mLin-7A expressed in COS7 cells (Figure 4A).

Since mLin-7B has been shown to be abundant in the cerebral cortex [23], we next investigated whether these RNAi vectors knocked down Lin-7B. Our results showed that mLin-7B was partially silenced by pSUPER–mLin7A#1, and hardly silenced by pSUPER–mLin7A#2 (Figure 4B). These results were expected based on the target sequence differences, and suggest that Lin-7B activity was partially maintained with the use of pSUPER-mLin7A#1, while almost completely maintained with pSUPER-mLin7A#2.

In the next set of experiments, the RNAi vectors and pCAG–EGFP were co-electroporated into progenitor cells in the ventricular zone (VZ) in the brains of embryonic mice, using *in utero* electroporation. Localization of transfected cells and their progeny was visualized at P2. In control experiments, vector-transfected neurons migrated normally to the superficial layer (layers II–IV) of the cortical plate (CP) (Figure 5A(a)). In contrast, a considerable portion of cells, which were transfected with pSUPER–mLin7A#1 or pSUPER–mLin7A#2, remained in the

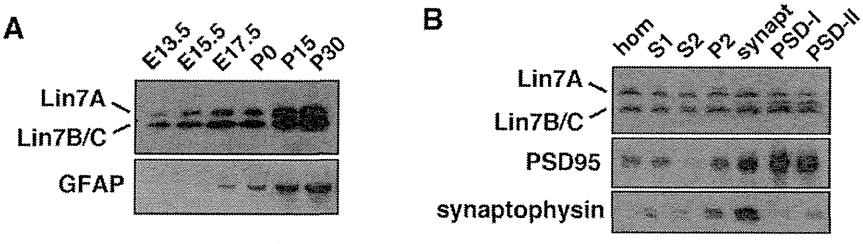

Figure 3. Expression profiles of Lin-7 proteins in the brain tissues. (**A**), Whole lysates (50 μg protein) of mouse cerebral cortices at various developmental stages were subjected to western blotting with antibodies against Lin-7 and GFAP. (**B**), Aliquots of brain fractions (10 μg) were immunoblotted with anti-Lin-7 (upper panel). hom, homogenate; S1, crude synaptosomal fraction; S2, cytosolic synaptosomal fraction; P2, crude synaptosomal pellet fraction; synapt, synaptosomal fraction; PSD-I, postsynaptic density fraction I; PSD-II, postsynaptic density fraction II. The blot was then re-probed with anti-PSD-95 (middle panel) and anti-synaptophysin (lower panel).
doi:10.1371/journal.pone.0092695.g003

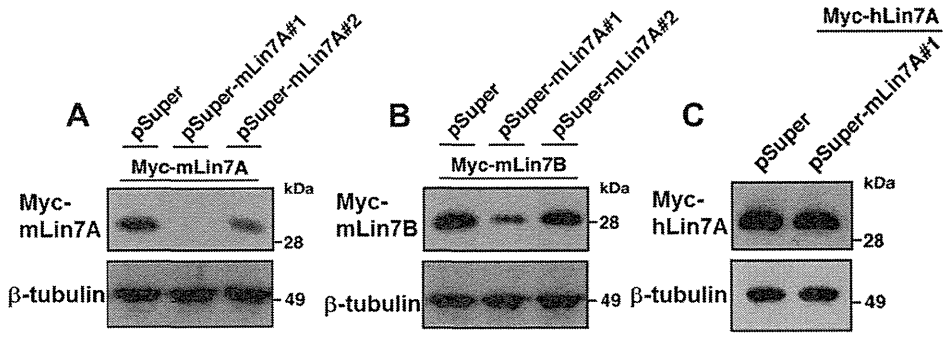

Figure 4. Characterization of RNAi vectors for Lin-7A. (**A**) pCAG-Myc-mLin-7A or (**B**) pCAG-Myc-mLin-7B was co-transfected into COS7 cells with control pSUPER vector, pSUPER–mLin7A#1, or pSUPER–mLin7A#2. After 48 h, cells were harvested and subjected to western blotting (20 μg protein per lane) with anti-Myc. Anti-β-tubulin was used as a loading control. (**C**), pCAG-Myc-hLin-7A was co-transfected into COS7 cells with control pSUPER vector or pSUPER–mLin7A#1. Analyses were done as in **A**.
doi:10.1371/journal.pone.0092695.g004

lower zone of the CP and the intermediate zone (IZ) (Figure 5A(b), (c)).

One-way ANOVA revealed significant effects of both vector injections [layers II–IV ($F2,6 = 333.167$, $P<0.001$); layers V–VI ($F2,6 = 95.746$, $P<0.001$); and IZ ($F2,6 = 248.152$ $P<0.001$)]. However, no significant effect was noted in the subventricular zone SVZ/VZ ($F2,6 = 0.8$, $P = 0.4919$). *Post-hoc* tests detected significant abnormal neuronal migration in cells that were injected with pSUPER–mLin7A#1 and #2 compared to control vector.

We next performed rescue experiments to rule out off-target effects. For this purpose, we used hLin-7A since it was resistant to pSUPER–mLin7A#1-mediated silencing (Figure 4C). When pCAG–EGFP and pSUPER–mLin7A#1 were co-electroporated together with pCAG–Flag-hLin7A, the positional defects by Lin-7A knockdown were rescued at P2 (Figure 5A(d)).

One-way ANOVA revealed significant effects of co-transfection with pCAG–Flag-hLin7A [layers II–IV ($F2,6 = 364.775$, $P<0.001$); layers V–VI ($F2,6 = 103.885$, $P<0.001$); and IZ ($F2,6 = 176.481$, $P<0.001$)]. However, no significant effects were observed in SVZ/VZ ($F2,6 = 0.892$, $P = 0.4578$). *Post-hoc* tests detected a significant rescue effect against abnormal neuronal migration. We then analyzed the effects of Lin-7A knockdown on

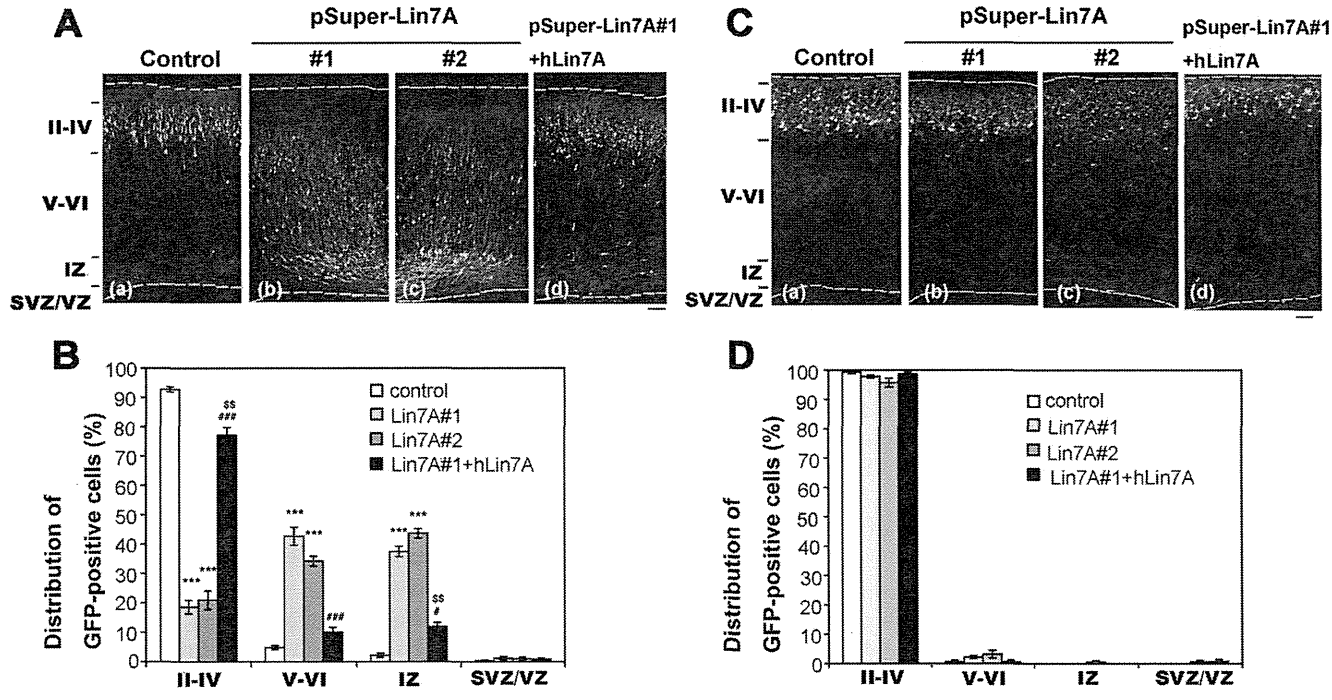

Figure 5. Role of Lin-7A in neuronal migration during corticogenesis. (**A**) and (**C**), pCAG-EGFP was co-electroporated with (a) pSUPER vector (Control), (b) pSUPER–mLin7A#1, or (c) pSUPER–mLin7A#2 into cerebral cortices at E14.5, and fixed at P2 (**A**) or P7 (**C**). Coronal sections were prepared and immunostained with polyclonal anti-GFP (white). Nuclei were stained with DAPI (blue). (**A**, d) Rescue of pSUPER–mLin7A#1-induced migration defects. pSUPER-mLin7A#1 was electroporated with pCAG-GFP and pCAG-Myc-hLin-7A into cerebral cortices at E14.5, followed by fixation at P2. Analyses were performed as described above. Bar, 100 μm. (**B**) and (**D**), Quantification of the distribution of GFP-positive cells in distinct regions of the cerebral cortex for each condition shown in **A** (**B**) and **C** (**D**). Values indicate the mean ± S.E.M. n = 3 each. $^{***}P<0.001$ vs. Control (Fisher's LSD test); $^{\#}P<0.05$, $^{\#\#\#}P<0.001$ vs. Lin7A#1 (Fisher's LSD test); $^{\$\$}P<0.01$ vs. Control (Fisher's LSD test).
doi:10.1371/journal.pone.0092695.g005

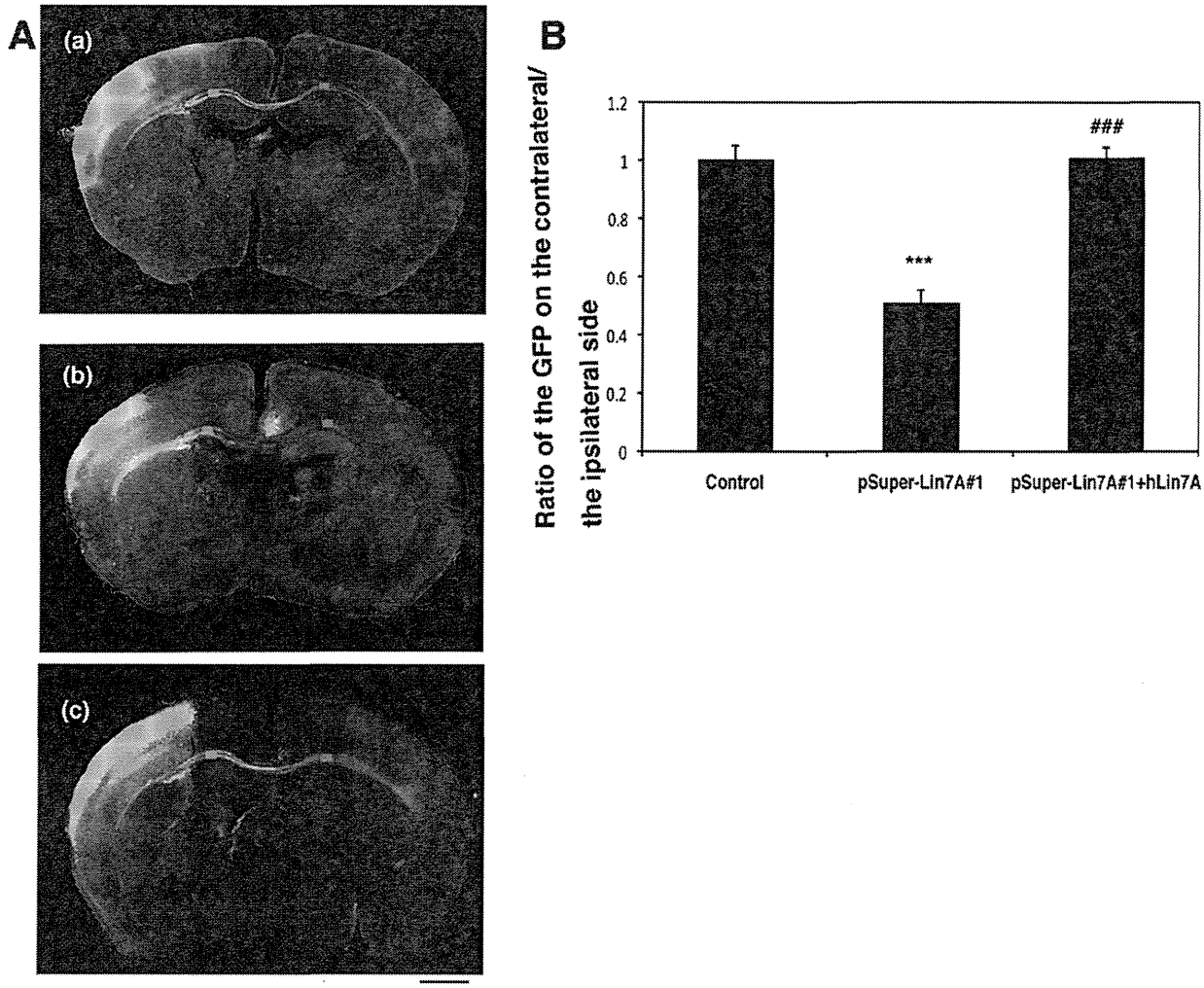

Figure 6. Role of Lin-7A in axon growth *ex vivo*. (**A**), Lin-7A deficiency affects the cortical axon growth. pCAG-EGFP was co-electroporated with (a) control pSUPER vector, (b) pSUPER-mLin7A#1, or (c) pSUPER-mLin7A#1+ hLin-7A into cerebral cortices at E14.5, and fixed at P7. Coronal sections were prepared and immunostained with polyclonal anti-GFP (white). Bar, 1 mm. (**B**), Quantitative analyses of the ratio of the intensity of GFP-positive axons in the area (green) of Lin-7A-deficient ipsilateral cortex to that in the area (red) of contralateral cortex in **A**. In the rescue experiments, hLin-7A was co-transfected as an RNAi-resistant version. Values indicate the mean ± S.E.M. n = 3 each. ***$P<0.001$ vs. Control (Fisher's LSD test); $^{\#\#\#}P<0.001$ vs. Lin7A#1 (Fisher's LSD test).
doi:10.1371/journal.pone.0092695.g006

the neuronal migration at P7. It should be noted that Lin7A-deficient cells reached the target location (layers II–IV) at this time point, indicating that silencing of Lin-7A delayed, but did not prevent, radial migration of cortical neurons (Figure 5C, D).

Lin-7A is not involved in the cell cycle of neuronal progenitor cells

Since a prolonged cell cycle is known to result in delayed neuronal migration [24], we next asked whether Lin-7A silencing affected the proliferation of neurons produced in the VZ. We examined the impact of Lin-7A silencing on cell proliferation in the VZ by labeling S-phase cells with 5-ethynil-2′-deoxyuridine (EdU) to detect DNA replication. We found that Lin-7A-deficient cells were able to enter S-phase to a similar extent as the control pSUPER-transfected cells (Figure S2A, B). Thus, the cell cycle G1-progression rate did not statistically differ between the control and Lin-7A-deficient cells, implying that Lin-7A knockdown did not affect cell division/proliferation at VZ and SVZ. Furthermore, the positioning of the EdU/EGFP double-positive cells within VZ and SVZ was not affected by Lin-7A knockdown (Figure S2A). Overall, we conclude that the cell cycle was not affected in Lin-7A-deficient cells, and that neuronal positioning defects by Lin-7A knockdown are attributable to an abnormality in cell migration rather than cell proliferation.

Role of Lin-7A in the interhemispheric connection of cortical neurons *in vivo*

Lin-7A deficiency could potentially affect not only cortical neuron migration but also axon path-finding, growth, and network formation during corticogenesis. Therefore, we analyzed inter-hemispheric axon projections of Lin-7A-deficient cortical neurons. To this end, we silenced Lin-7A in VZ progenitor cells at E14.5, and visualized axons in the contralateral hemisphere at P7.

We found that, compared to the control cells, approximately half of the axons of Lin-7A-deficient neurons were disrupted from entering the contralateral hemisphere after leaving the corpus callosum (Figure 6A(a), (b), B). This phenotype was rescued by exogenous expression of hLin-7A (Figure 6A(c), B). These results

suggest that Lin-7A is required for axon growth of excitatory neurons from the ipsilateral cortex to the contralateral cortex, the disturbance of which leads to hypoplasia of the corpus callosum.

Discussion

The clinical features of 12q21 deletion that were shared by the four previously reported patients [1–4] and our patient include ID, low-set ears, sparse hair, prominent forehead, and hyper- or hypotelorism (Table S1). Additionally, short upturned nose, small mandible, ocular abnormality, cardiac abnormality, and chronic dermatitis were each observed in three to four cases. Neuroimaging detected ventriculomegaly in three cases [1,3], delayed myelination in one case [1], and mild hypoplasia of the corpus callosum in our present case. Our present case also involved sleep disturbance. These symptoms and signs, which we observed in this patient, can be considered phenotypes of 12q21 deletion, since there have only been a few reported patients, and the features of 12q21 deletion have not been established.

The previously reported cases of 12q21 deletion were analyzed by G-banding [1,4] and array CGH with BAC clones [2,3]. The deletion in the present case, from 12q21.2 to 12q21.33 (77.2–91.2 Mb), was the shortest and most definitively detected deletion in any of the five cases, suggesting that this region contains the gene(s) responsible for the concordant features (Figure 2C). Our patient also had the inversion of 12q13.1–q21.2. ZDHHC17 was disrupted on one side of the deletion, while no gene exists on the other side of the deletion. Information about the other end of inversion was not obtained; we do not deny the possibility that the disrupted ZDHHC17 or putative gene on the other side of the inversion could have gained some function in addition to the loss of function.

The present study provided evidence that functional defects of Lin-7A may be involved in the pathophysiology of 12q21-deletion syndrome, possibly through impaired cerebral development. Although molecular mechanisms governing the pathophysiology are enigmatic, we assume that Lin-7A participates in neuronal migration during corticogenesis. It should be noted here that the migration delay of Lin-7A-deficient neurons at P2 was recovered at P7, and these cells eventually arrived at their correct destination.

While migration abnormality has not been reported in the 12q21 deletion syndrome. It is, however, likely that the delayed migration process *per se* may cause deficiency in neuronal functions, leading to ID in 12q21-deletion syndrome. Interestingly, comparable phenotypes have been observed in the course of pathophysiological analyses of *SIL1*, a causative co-chaperone gene of Marinesco-Sjogren syndrome, in which ID is a major symptom [25].

Characteristic phenotypes were not observed in the cerebral cortex of Lin-7A/B-knockout mice [23]. Notably, up-regulation of Lin-7C was observed in the knockout mouse, and, thus, may compensate for the knockout phenotype. On the other hand, acute knockdown by *in utero* electroporation is suggested to circumvent the compensatory effects of general gene-knockout approaches. In this context, a scaffold protein Doublecortin- or a cytoskeleton-related molecule, Sept4-deficient mice also exhibited no obvious morphological alteration in the cerebral cortex [26,27], while acute knockdown of these genes by *in utero* electroporation resulted in defective neuronal migration [21,28].

The corpus callosum was hypoplastic in our present 12q21-deletion syndrome case. The corpus callosum consists of more than 200 million axons, which originate from neurons of layers II, III, and V of the cerebral cortex [29,30]. Given that axons from the hemisphere containing Lin-7A-deficient neurons did not efficiently extend into the contralateral cortex, the hypoplasia of the corpus callosum in our proband is likely attributable to defects in Lin-7A function.

LIN7A is known to relate to synaptic functions [10,11]. Here we clarified that Lin-7A was enriched in synapses, and played a pivotal role in cortical neuron migration and axon network formation during corticogenesis. Although neuronal migration defects were temporal, and neurons eventually located at their correct positions, loss of function of Lin-7A should cause a subtle abnormal architecture of the developing cerebral cortex, leading to dysfunction of synapses and/or axon growth. Overall, our results indicate that the ID and hypoplasia of the corpus callosum observed in our 12q21-deletion syndrome case may be the phenotype of *Lin7A* deletion.

Supporting Information

Figure S1 Chromosome 12 analysis by a highly accurate technique. Arrows indicate the inversion of q13.1q21.2. The blue line next to the inversion area indicates the deletion of q21.2q21.3.
(TIF)

Figure S2 Effects of Lin7A silencing on the DNA replication in S-phase of the cell cycle. (**A**), E14 cortices were co-electroporated with pCAG-EGFP together with control pSUPER vector or pSUPER–mLin7A#1. Coronal sections were visualized for GFP (green) and EdU (red). Arrowheads indicate EdU/GFP double-positive cells. Dotted lines represent ventricular surface. Bars, 50 μm. (**B**), Quantification of EdU/EGFP double-positive cells among EGFP-positive cells. Values indicate the mean ± S.E.M. n = 3 each.
(TIF)

Table S1 Clinical features of 12q21 deletion syndrome.
(DOCX)

Author Contributions

Conceived and designed the experiments: EFJ MYM KN TY. Performed the experiments: AM MM NH YN. Analyzed the data: AM MM KN TY. Contributed reagents/materials/analysis tools: AM MM NH YN KN TY. Wrote the paper: AM MM KN TY.

References

1. Rauen KA, Cotter PD, Bitts SM, Cox VA, Golabi M (2000) Cardio-facio-cutaneous syndrome phenotype in an individual with an interstitial deletion of 12q: identification of a candidate region for CFC syndrome. Am J Med Genet 93: 219–222.
2. Rauen KA, Albertson DG, Pinkel D, Cotter PD (2002) Additional patient with del(12)(q21.2q22): further evidence for a candidate region for cardio-facio-cutaneous syndrome? Am J Med Genet 110: 51–56.
3. Klein OD, Cotter PD, Schmidt AM, Bick DP, Tidyman WE, et al. (2005) Interstitial deletion of chromosome 12q: genotype-phenotype correlation of two patients utilizing array comparative genomic hybridization. Am J Med Genet A 138: 349–354.
4. Brady AF, Elsawi MM, Jamieson CR, Marks K, Jeffery S, et al. (1999) Clinical and molecular findings in a patient with a deletion on the long arm of chromosome 12. J Med Genet 36: 939–941.
5. Niihori T, Aoki Y, Narumi Y, Neri G, Cave H, et al. (2006) Germline KRAS and BRAF mutations in cardio-facio-cutaneous syndrome. Nat Genet 38: 294–296.
6. Guilmatre A, Dubourg C, Mosca AL, Legallic S, Goldenberg A, et al. (2009) Recurrent rearrangements in synaptic and neurodevelopmental genes and shared biologic pathways in schizophrenia, autism, and mental retardation. Arch Gen Psychiatry 66: 947–956.

7. Humeau Y, Gambino F, Chelly J, Vitale N (2009) X-linked mental retardation: focus on synaptic function and plasticity. J Neurochem 109: 1–14.
8. Zheng CY, Seabold GK, Horak M, Petralia RS (2011) MAGUKs, synaptic development, and synaptic plasticity. Neuroscientist 17: 493–512.
9. Feng W, Zhang M (2009) Organization and dynamics of PDZ-domain-related supramodules in the postsynaptic density. Nat Rev Neurosci 10: 87–99.
10. Jo K, Derin R, Li M, Bredt DS (1999) Characterization of MALS/Velis-1, -2, and -3: a family of mammalian LIN-7 homologs enriched at brain synapses in association with the postsynaptic density-95/NMDA receptor postsynaptic complex. J Neurosci 19: 4189–4199.
11. Butz S, Okamoto M, Sudhof TC (1998) A tripartite protein complex with the potential to couple synaptic vesicle exocytosis to cell adhesion in brain. Cell 94: 773–782.
12. Lanktree M, Squassina A, Krinsky M, Strauss J, Jain U, et al. (2008) Association study of brain-derived neurotrophic factor (BDNF) and LIN-7 homolog (LIN-7) genes with adult attention-deficit/hyperactivity disorder. Am J Med Genet B Neuropsychiatr Genet 147B: 945–951.
13. Shinawi M, Sahoo T, Maranda B, Skinner SA, Skinner C, et al. (2011) 11p14.1 microdeletions associated with ADHD, autism, developmental delay, and obesity. Am J Med Genet A 155A: 1272–1280.
14. Zucker B, Kama JA, Kuhn A, Thu D, Orlando LR, et al. (2010) Decreased Lin7b expression in layer 5 pyramidal neurons may contribute to impaired corticostriatal connectivity in huntington disease. J Neuropathol Exp Neurol 69: 880–895.
15. Sudo K, Ito H, Iwamoto I, Morishita R, Asano T, et al. (2006) Identification of a cell polarity-related protein, Lin-7B, as a binding partner for a Rho effector, Rhotekin, and their possible interaction in neurons. Neurosci Res 56: 347–355.
16. Nagata K, Kawajiri A, Matsui S, Takagishi M, Shiromizu T, et al. (2003) Filament formation of MSF-A, a mammalian septin, in human mammary epithelial cells depends on interactions with microtubules. J Biol Chem 278: 18538–18543.
17. Mizutani Y, Ito H, Iwamoto I, Morishita R, Kanoh H, et al. (2013) Possible role of a septin, SEPT1, in spreading in squamous cell carcinoma DJM-1 cells. Biol Chem 394: 281–290.
18. Ito H, Atsuzawa K, Morishita R, Usuda N, Sudo K, et al. (2009) Sept8 controls the binding of vesicle-associated membrane protein 2 to synaptophysin. J Neurochem 108: 867–880.
19. Tabata H, Nakajima K (2001) Efficient in utero gene transfer system to the developing mouse brain using electroporation: visualization of neuronal migration in the developing cortex. Neuroscience 103: 865–872.
20. Nishimura YV, Shinoda T, Inaguma Y, Ito H, Nagata K (2012) Application of in utero electroporation and live imaging in the analyses of neuronal migration during mouse brain development. Med Mol Morphol 45: 1–6.
21. Shinoda T, Ito H, Sudo K, Iwamoto I, Morishita R, et al. (2010) Septin 14 is involved in cortical neuronal migration via interaction with Septin 4. Mol Biol Cell 21: 1324–1334.
22. Reiner O, Sapir T (2009) Polarity regulation in migrating neurons in the cortex. Mol Neurobiol 40: 1–14.
23. Misawa H, Kawasaki Y, Mellor J, Sweeney N, Jo K, et al. (2001) Contrasting localizations of MALS/LIN-7 PDZ proteins in brain and molecular compensation in knockout mice. J Biol Chem 276: 9264–9272.
24. Ayala R, Shu T, Tsai LH (2007) Trekking across the brain: the journey of neuronal migration. Cell 128: 29–43.
25. Inaguma Y, Hamada N, Tabata H, Iwamoto I, Mizuno M (2014) SIL1, a causative cochaperone gene of Marinesco-Sjogren syndrome, plays an essential role in establishing the architecture of the developing cerebral cortex. EMBO Mol Med in press.
26. Corbo JC, Deuel TA, Long JM, LaPorte P, Tsai E, et al. (2002) Doublecortin is required in mice for lamination of the hippocampus but not the neocortex. J Neurosci 22: 7548–7557.
27. Ihara M, Yamasaki N, Hagiwara A, Tanigaki A, Kitano A, et al. (2007) Sept4, a component of presynaptic scaffold and Lewy bodies, is required for the suppression of alpha-synuclein neurotoxicity. Neuron 53: 519–533.
28. Bai J, Ramos RL, Ackman JB, Thomas AM, Lee RV, et al. (2003) RNAi reveals doublecortin is required for radial migration in rat neocortex. Nat Neurosci 6: 1277–1283.
29. Wise SP (1975) The laminar organization of certain afferent and efferent fiber systems in the rat somatosensory cortex. Brain Res 90: 139–142.
30. Zhou J, Wen Y, She L, Sui YN, Liu L, et al. (2013) Axon position within the corpus callosum determines contralateral cortical projection. Proc Natl Acad Sci U S A 110: E2714–2723.

ELSEVIER

Brain & Development xxx (2013) xxx–xxx

BRAIN & DEVELOPMENT
Official Journal of the Japanese Society of Child Neurology

www.elsevier.com/locate/braindev

Case report

Williams–Beuren syndrome with brain malformation and hypertrophic cardiomyopathy

Noriko Okamoto [a], Takanori Yamagata [a,*], Yukari Yada [a], Ko Ichihashi [a], Naomichi Matsumoto [b], Mariko Y. Momoi [a], Takeshi Mizuguchi [b]

[a] *Department of Pediatrics, Jichi Medical University, Japan*
[b] *Department of Human Genetics, Yokohama City University Graduate School of Medicine, Japan*

Received 3 March 2013; received in revised form 7 June 2013; accepted 4 July 2013

Abstract

Williams–Beuren syndrome (WBS) is a multisystemic genetic disorder caused by a contiguous gene deletion at 7q11.23. We report a severely affected WBS patient with cerebral and cerebellar dysplasia as well as hypertrophic cardiomyopathy. Microarray comparative genomic hybridization (aCGH) detected a deletion on 7q11.23 expanding from RP11-614D7 to RP11-137E8, which is a typical deletion in WBS. To the best of our knowledge, this is the first case report of a WBS patient with severe congenital central nervous system anomaly and progressive hypertrophic cardiomyopathy. The relationship between the genes deleted in WBS and a CNS anomaly plus hypertrophic cardiomyopathy requires further analysis.

Keywords: Williams syndrome; Cerebral and cerebellar dysplasia; Hypertrophic cardiomyopathy; Microarray comparative genomic hybridization analysis (aCGH)

1. Introduction

Williams–Beuren syndrome (WBS) is caused by a hemizygous deletion of chromosome 7q11.23 [1]. Phenotypes consist of characteristic facies, cardiovascular abnormalities, infantile hypercalcemia, growth deficiency, and intellectual disability. About 80% of patients have cardiovascular abnormalities, and supravalvular aortic stenosis (SVAS) is a characteristic feature [2]. With regard to neurological symptoms, mild microcephaly, intellectual disability, and personality disorders are common [3]. We report a patient with the common WBS deletion in 7q11.23 presenting with severe cerebral and cerebellar dysplasia and progressive hypertrophic cardiomyopathy. These phenotypes have not been previously reported.

2. Case report

The patient was born at 35 weeks of gestation with a weight of 2.294 kg (−0.16 standard deviation (SD)), a height of 42.5 cm (−1.2 SD), and a head circumference of 35.4 cm (+2.5 SD). The patient's dyspnea was controlled with mechanical ventilation. He had blepharophimosis, downward slanting of the palpebral fissure, strabismus, right iris hypopigmentation, a left pupillary membrane remnant, low-set ears, high-arched palate, periorbital fullness, broad nose, thick lips, wide mouth, micrognathia, loose skin, hypoplastic right toes with nail aplasia, deviation of the left second digit, and contracture of hip and knee joints. His voice was deep and

* Corresponding author. Address: Department of Pediatrics, Jichi Medical University School of Medicine, 3311-1, Yakushiji, Shimotsuke, Tochigi 329-0498, Japan. Tel.: +81 285 58 7366; fax: +81 285 44 6123.
E-mail address: takanori@jichi.ac.jp (T. Yamagata).

0387-7604/$ - see front matter © 2013 The Japanese Society of Child Neurology. Published by Elsevier B.V. All rights reserved.
http://dx.doi.org/10.1016/j.braindev.2013.07.002

husky. Echocardiography on the day of birth revealed a small ventricular septal defect (VSD). At 1 month of age, right ventricular hypertrophy progressed and right ventricle outlet stenosis was detected. At 2 months of age, left ventricular hypertrophy and left ventricle output stenosis gradually progressed and severe mitral valve insufficiency was observed (Fig. 1d and e). Magnetic resonance imaging (MRI) at day 1 and day 81 after birth, and cranial computed tomography (CT) at 2 weeks of age showed dilatation of lateral and third ventricles, indicative of congenital hydrocephalus, thin cerebral cortex, hypoplasia of the cerebellum and brain stem, and agenesis of the corpus callosum (Fig. 1a–c). Beginning at 3 months of age, the patient had generalized tonic convulsions several times each day. Laboratory evaluation on the day of birth revealed mild hypocalcemia (7.8 mg/dl) and low blood sugar (34 mg/dl); both promptly improved with an intravenous infusion. Hypothyroidism was detected (free thyroxine (T4) 0.34 ng/dl (normal: 0.96–1.79 ng/dl); free triiodothyronine (T3) 1.18 pg/ml (normal: 2.47–4.34 pg/ml); and thyroid-stimulating hormone (TSH) 83.71 μIU/ml (normal: 0.34–3.5 μIU/ml)); thyroid hormone supplementation was initiated. His karyotype by G-banding was 46, XY. The auditory brainstem response showed bilateral hearing difficulties with the right threshold at 85 decibels (dB) and the left threshold at 105 dB. The patient died at 1 year and 5 months of age due to heart failure. At that time, his weight was 5.25 kg (−4.3 SD) and his height was 64 cm (−5.2 SD).

3. Materials and methods

3.1. Microarray CGH analysis (aCGH)

Comparative genomic hybridization analysis was performed using a custom BAC microarray containing 4219 BAC clones, as previously described [4]. In brief, after complete digestion using Dpn II, the subject's DNA was labeled with Cy-5 deoxycytidine triphosphate

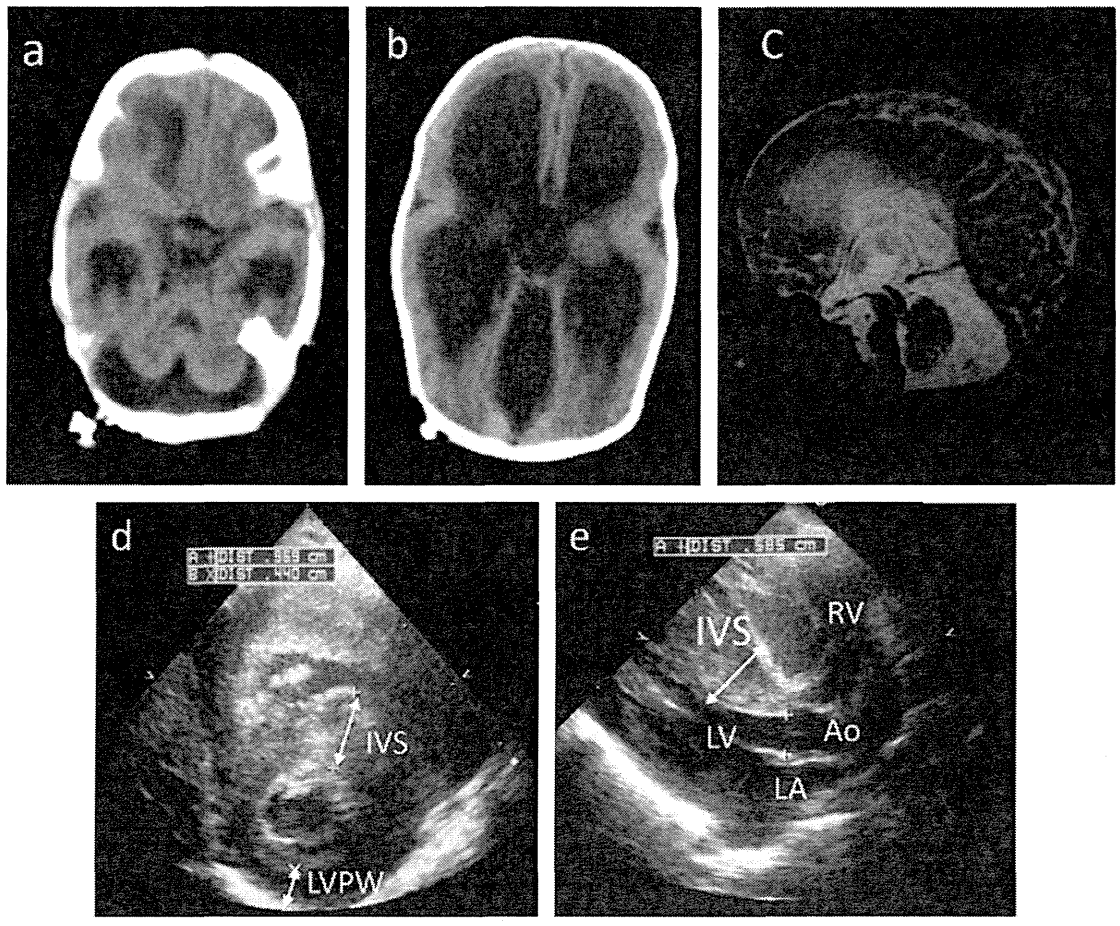

Fig. 1. Brain neuroimagings and echocardiogram. (1) Brain CT at 2 weeks of age (a, b) and T2-weighted imaging on MRI at day 1 (c) revealed dilated lateral and third ventricles, thin cerebral cortex, cerebellar hypoplasia, hypoplasia of brain stem, and agenesis of the corpus callosum. (2) Echocardiogram at 2 months of age (d, e) revealed hypertrophic obstructive cardiomyopathy with severe left ventricular outflow tract obstruction. Arrow indicates a markedly enlarged intraventricular septum (IVS). LVPW: posterior wall of left ventricle; LV: left ventricle; RV: right ventricle; LA: left atrium; Ao: aorta.

Please cite this article in press as: Okamoto N et al. Williams–Beuren syndrome with brain malformation and hypertrophic cardiomyopathy. Brain Dev (2013), http://dx.doi.org/10.1016/j.braindev.2013.07.002

(dCTP), and reference DNA was labeled with Cy-3 dCTP (Amersham Biosciences, Piscataway, NJ). Hybridization steps for array were preformed on a Tecan hybridization station HS400 (Tecan Japan, Kawasaki, Japan). Arrays were scanned by GenePix 4000B (Axon Instruments, Union City, CA) and analyzed using GenePix Pro 6.0 (Axon Instruments). The signal intensity ratio between patient and control DNA was calculated from the data of the single-slide experiment using the ratio of means formula (F635 mean − B635 median/F532 mean − B532 median) according to GenePix Pro 6.0. The standard deviation was calculated from the data of all clones.

3.2. Fluorescence in situ hybridization (FISH)

BAC DNAs, RP11-805G2 and RP11-359E24 were labeled with SpectrumGreen™ -11-deoxyuridine triphosphate (dUTP) or SpectrumOrange™ -11-dUTP (Vysis, Downers Grove, IL) by nick translation and denatured at 70 °C for 10 min. Probe-hybridization mixtures (15 l l) were applied to the chromosomes, incubated at 37 °C for 16 h, then washed and mounted in antifade solution (Vector, Burlingame, CA) containing 4′-6′-diamidino-2-phenylindole.

These analyses were approved by the Bioethics Committee for human gene analysis at Jichi Medical University and Yokohama City University, and were performed after informed consent of patient's parents.

4. Results

With aCGH, a unique abnormality was detected: an approximate 1.0-Mb deletion in 7q11.23, ranging from RP11-614D7 (72,182,285–72,371,583) to RP11-137E8 (73,389,371–73,574,238) (Fig. 2a). This deletion range is commonly found in WBS. With FISH analysis, BAC clone RP11-805G2, which located within the deleted region, showed no signal on one of the 7q chromosome of the patient's lymphocytes. Instead, RP11-359E24, which located outside of the deletion, showed a signal (Fig. 2b). The patient's parents did not have

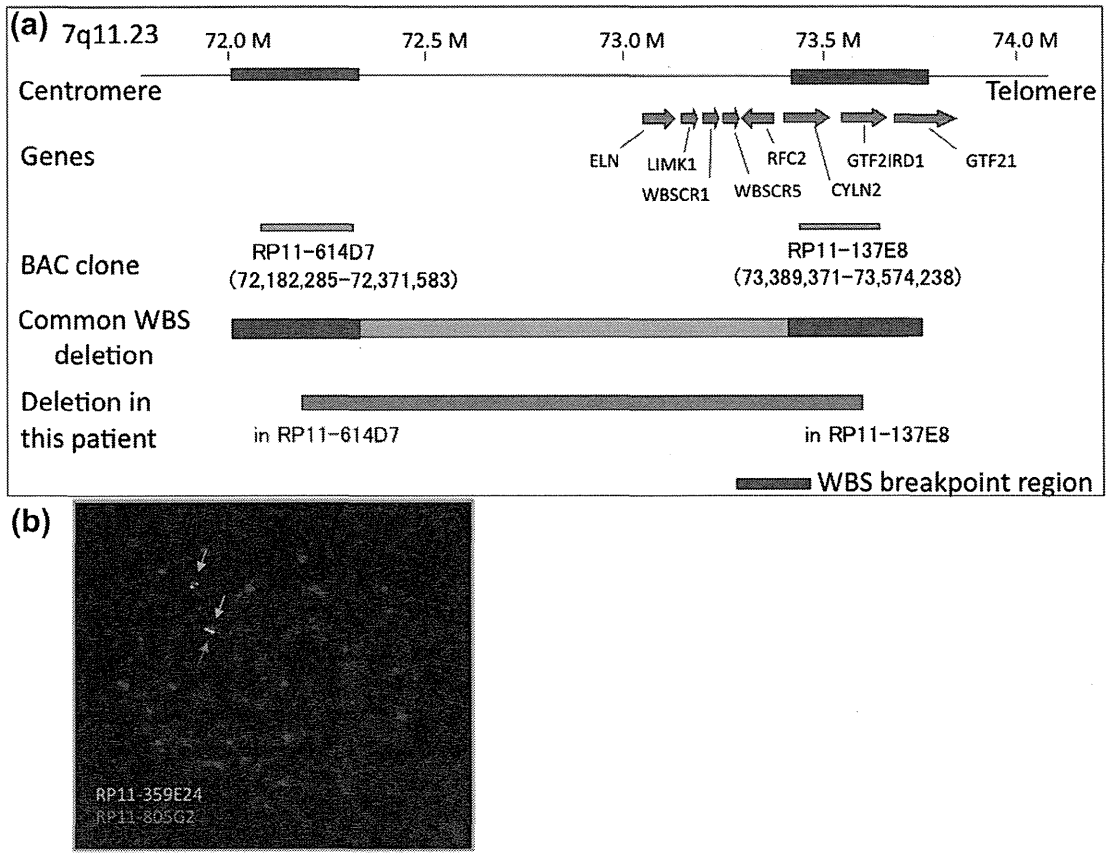

Fig. 2. (a) The range of the deletion detected in this case. Diagram presents a range of the common WBS deletion region and genes located nearby. The bar in the bottom indicates the extent of the deletion. In this case, aCGH detected the deletion expanding from RP11-614D7 to RP11-137E8. This interval of deletion is typical for WBS. (b) FISH analysis FISH results using BAC clone RP11-805G2 (red signal) localized in the common WBS deletion and RP11-359E24 (green signal) that is located outside of the deletion on chromosome 7 as probes. Our case had one normal chromosome 7 showing both green and red signals, and one chromosome 7 with a deletion missing a red signal. (For interpretation of the references to color in this figure legend, the reader is referred to the web version of this article.)

Please cite this article in press as: Okamoto N et al. Williams–Beuren syndrome with brain malformation and hypertrophic cardiomyopathy. Brain Dev (2013), http://dx.doi.org/10.1016/j.braindev.2013.07.002

Table 1
Clinical features of Williams Syndrome and our case.

Organ system	Problem	Williams syndrome	Our case
Facial	Combination of flat midface	Common	+
	Broad and depressed nasal bridge	CommonCommon	++
	Anteverted nares	Common	+
	Long philtrum	Common	+
	Thick lips	–	+
	High-arched palateLow-set ear	–	+
Ocular	Short palpebral fissures	50%	+
	Iris pigment abnormality	77%	+
	Strabismus	50%	+
Cardiovascular	Supravalvular aortic stenosis	64%	–
	Supravalvular pulmonic stenosis	24%	–
	Ventricular septal detect	12%5%	+–
	Patent ductus arteriosus	–	+
	Hypertrophic cardiomyopathy		
Central nervous system	Mild microcephaly	35%	–
	Mental retardation	95%	+
	Hypersensitivity to sound	90%	–
	Cerebellar hypoplasia	–	+
	Cerebral hypoplasia	–	+
	Infantile spasms	Rare	+
Musculoskeletal	Joint limitation	50%	+
	Joint contractures	Common	+
	Shift adhesion of digit	–	+
Gastrointestinal	Constipation	43%	–
Genitourinary	Renal artery narrowing	44%	–
Endocrine	Hypothyroidism	25%	+
Other findings	Hypoplastic, deeply set nails	65%	+
	Inguinal hernia	38%	+
	Umbilical hernia	14%	–
	Hypercalcemia	15%	–
	Hearing difficulties	NS	+

Modified from CA Morris et al. (1998) [2] and RJ Gorlin et al. (2001) [3]. +: present; –: absent.

the same deletion when tested by FISH analysis (data not shown).

5. Discussion

Clinical features of typical WBS and this case are compared in Table 1. Most of the common features of WBS were also observed in this case. In addition to these, some rare phenotypes of WBS, such as hearing difficulty and hypothyroidism [5], were detected. Conversely, SVAS, which is the most common cardiac anomaly associated with WBS [6], was not observed. Our patient developed rapidly progressing hypertrophic cardiomyopathy beginning at 2 months of age. A cardiomyopathy associated with WBS has been reported in only one 36-year-old patient [7], and severe hypertrophic cardiomyopathy has not been previously reported.

In addition, our patient exhibited the central nervous system (CNS) anomaly of congenital hydrocephalus and cerebral/cerebellar hypoplasia. Intellectual disabilities and behavioral problems are features of WBS; however, a CNS anomaly has not been previously noted as a clinical feature of WBS. Chiari I malformation has been reported in a small number of individuals with WBS [8], and parieto-occipital structural abnormality that might relate to visuospatial construction has been reported [9]. Schmitt et al. [10] reported that the midline lengths of the cerebral hemisphere and the corpus callosum were decreased in patients with WBS and suggested that the brain findings are consistent with aberrant premature termination of brain development. This proposed mechanism of premature termination of brain development might have occurred to a severe degree in this patient.

The extent of the deletion detected in this patient was typical of WBS; therefore, other specific genes that could explain these anomalies were not deleted. The possibility of the existence of some other gene mutation(s) in the homologous allele of the deleted region or outside of the deletion was not eliminated. It is possible that these anomalies could be features of WBS. There may be patients who remain undiagnosed because these features are atypical, and severe inducing early death. The relationships between the deleted genes in WBS and CNS anomalies as well as hypertrophic cardiomyopathies require further analysis.

Please cite this article in press as: Okamoto N et al. Williams–Beuren syndrome with brain malformation and hypertrophic cardiomyopathy. Brain Dev (2013), http://dx.doi.org/10.1016/j.braindev.2013.07.002

Acknowledgement

This work was supported in part by research grants from the Ministries of Education, Science and Culture, Japan.

References

[1] Nickerson E, Greenberg F, Keating MT, McCaskill C, Shaffer LG. Deletions of the elastin gene at 7q11.23 occur in approximately 90% of patients with Williams syndrome. Am J Hum Genet 1995;56:1156–61.

[2] Morris CA, Dilts C, Demsey SA, Leonard CO, Dilts C, Blackburn BL. The natural history of Williams syndrome: physical characteristics. J Pediatr 1988;113:318–26.

[3] Gorlin RJ, Cohen Jr MM, Hennekam RM. Syndromes of the head and neck. USA: Oxford University Press; 2001. p. 1032–8.

[4] Saitsu H, Kato M, Mizuguchi T, Hamada K, Osaka H, Tohyama J, et al. De novo mutations in the gene encoding STXBP1 (MUNC18-1) cause early infantile epileptic encephalopathy. Nat Genet 2008;40:782–8.

[5] Lashkari A, Smith AK, Graham JM. Williams–Beuren syndrome: an update and review for the primary physician. Clin Pediatr Phila 1999;38:189–208.

[6] Wessel A, Pankau R, Berdau W, Loens P. Aortic stiffness with the Williams–Beuren syndrome. Pediatr Cardiol 1997;18:244.

[7] Mäuser WS, Bonnemeier H. Cardiomyopathy and sudden cardiac death in Williams–Beuren syndrome. Int J Cardiol 2012;156:53–4.

[8] Pober BR, Filiano JJ. Association of Chiari I malformation in Williams syndrome. Pediatr Neurol 1995;12:84–8.

[9] Boddaert N, Mochel F, Meresse I, Seidenwurm D, Cachia A, Brunelle F, et al. Parieto-occipital grey matter abnormalities in children with Williams syndrome. Neuro Image 2006;30:721–5.

[10] Schmitt JE, Eliez S, Bellugi U, Reiss AL. Analysis of cerebral shape in Williams syndrome. Arch Neurol 2001;58:283–7.

Hindawi Publishing Corporation
BioMed Research International
Volume 2013, Article ID 974819, 8 pages
http://dx.doi.org/10.1155/2013/974819

Research Article

Systemic Delivery of Tyrosine-Mutant AAV Vectors Results in Robust Transduction of Neurons in Adult Mice

Asako Iida,[1] Naomi Takino,[1] Hitomi Miyauchi,[1] Kuniko Shimazaki,[2] and Shin-ichi Muramatsu[1]

[1] *Division of Neurology, Department of Medicine, Jichi Medical University, 3311-1 Yakushiji, Shimotsuke, Tochigi 329-0498, Japan*
[2] *Division of Neurosurgery, Jichi Medical University, 3311-1 Yakushiji, Shimotsuke, Tochigi 329-0498, Japan*

Correspondence should be addressed to Shin-ichi Muramatsu; muramats@jichi.ac.jp

Received 6 February 2013; Revised 19 April 2013; Accepted 21 April 2013

Academic Editor: Akhtar Jamal Khan

Recombinant adeno-associated virus (AAV) vectors are powerful tools for both basic neuroscience experiments and clinical gene therapies for neurological diseases. Intravascularly administered self-complementary AAV9 vectors can cross the blood-brain barrier. However, AAV9 vectors are of limited usefulness because they mainly transduce astrocytes in adult animal brains and have restrictions on foreign DNA package sizes. In this study, we show that intracardiac injections of tyrosine-mutant pseudotype AAV9/3 vectors resulted in extensive and widespread transgene expression in the brains and spinal cords of adult mice. Furthermore, the usage of neuron-specific promoters achieved selective transduction of neurons. These results suggest that tyrosine-mutant AAV9/3 vectors may be effective vehicles for delivery of therapeutic genes, including miRNAs, into the brain and for treating diseases that affect broad areas of the central nervous system.

1. Introduction

Various gene delivery carriers have been tested in preclinical gene therapies for diseases that affect the central nervous system (CNS). Based on the results of these studies, adeno-associated virus (AAV) derived vectors are the most suitable for clinical applications because they are both efficacious and safe [1–3]. Infusions of recombinant AAV vectors via stereotaxic surgeries into target brain areas result in continuous and long-term expression of transgenes [4, 5]. Several phase I/II gene therapy trials for Parkinson's disease, in which therapeutic genes were introduced into the putamen or subthalamic nucleus, demonstrate encouraging clinical benefits [5–8]. However, for diseases that affect large areas of the CNS, such as Alzheimer's disease, lipid storage diseases, and multiple sclerosis, local injections of the vectors yield suboptimal results. Vector deliveries through the vasculature system may achieve more widespread transductions of the viruses.

Vectors derived from AAV type 9 (AAV9) have recently become popular because they cross the blood-brain barrier (BBB) or the blood-cerebrospinal fluid barrier [9–14]. However, while intravenous injections of AAV9 vectors achieved efficient transduction of spinal motor neurons in fetal, neonate, and adult mice, as well as in adult cats and pigs [9–13, 15, 16], most of the transduced cells were astrocytes in adult mice and nonhuman primates [9, 14, 16]. Thus, extensive gene delivery to neurons in the adult CNS remains challenging.

Most previous reports about systemic delivery of AAV9 vectors to the CNS used self-complementary AAV (scAAV) vectors with two complementary copies of a transgene that were inserted at the expense of maintaining small packaging sizes (less than 2.2 kb) [17]. scAAV vectors are 20- to 100-fold more efficient than conventional single strand AAV vectors [18], but packaging constraints set strict size limits on the genes that can be delivered. Furthermore, AAV9 vectors with a cytomegalovirus (CMV) promoter can transduce antigen-presenting cells in the brain and provoke an adaptive immune response that results in significant brain pathology [19]. This immune response presents an additional obstacle for the usage of AAV9 vectors in the CNS. Usage of neuron-specific promoters

may circumvent this strong immune reaction. However, many cell-type specific promoters drive relatively weak gene expression [20]. Therefore, we devised a novel approach in order to improve transgene expression. Specifically, we eliminated two surface-exposed tyrosine residues from the capsid protein of AAV9. Substituting highly conserved surface-exposed capsid tyrosine residues for phenylalanine residues results in increased infectivities for several AAV vectors [21–27]. Our results in this study demonstrate that tyrosine-mutant pseudotype AAV9/3 vectors with neuron-specific promoters can achieve extensive gene expression in neurons.

2. Materials and Methods

2.1. Generation of Pseudotype AAV9/3 Vectors. The AAV vector plasmids contained an expression cassette consisting of a promoter, which was followed by cDNA encoding either green fluorescent protein (GFP) or the microRNA (miRNA) sequence for human aromatic L-amino acid decarboxylase (AADC) and then a woodchuck hepatitis virus posttranscriptional regulatory element. The expression cassette was located between the inverted terminal repeats of the AAV type 3 (AAV3) genome. Three distinct promoters were used: a human cytomegalovirus immediate-early enhancer and chicken β-actin (CAG) promoter, the neuron-specific synapsin I promoter (Gene Bank, M55300.1) [28], or the Purkinje cell-specific L7 promoter (Gene Bank, S40022.1) [29]. A double strand DNA sequence encoding the miRNA for human AADC was synthesised with the following sequence: 5′-TGCTGAATTCAGGACAGATAAAGGCAGTTTTGGCCACTGACTGACTGCCTTTATGTCCTGAATT-3′. The AAV9 *vp* cDNA was synthesised as previously described [30], except that substitutions of thymidine for adenine were inserted at positions 1337 and 2192. These substitutions introduced amino acid changes from tyrosine to phenylalanine at positions 446 and 731. The recombinant AAV vectors were produced by transient transfection of HEK293 cells, as previously described [31]. The cells were transfected with the vector plasmid, the AAV3 *rep* and AAV9 *vp* expression plasmids, and the adenoviral helper plasmid pHelper (Invitrogen). The recombinant viruses were purified by isolation from two sequential continuous CsCl gradients. Finally, the viral titers were determined by qRT-PCR.

2.2. Intracardiac Vector Injections in Adult Mice. All animal experiments were performed in compliance with institutional guidelines. Twenty-four male, C57BL/6, 9-10-week-old mice were included in this study. The mice were housed in plastic cages, had ad lib access to food and water, and were maintained on a 12/12 h light-dark cycle. For injections, AAV vectors were diluted in phosphate-buffered saline (PBS) to 1.2×10^{11}–8.5×10^{12} vectors genome/100 μL. Mice were anaesthetised with pentobarbital (50 mg/kg, ip), and then 100 μL of the diluted AAV vectors was intracardially injected with a 0.5 mL syringe equipped with a 29-gauge needle.

2.3. Immunohistochemistry. Four to eight weeks after injections of vectors, the mice were anaesthetised with pentobarbital and perfused with ice-cold 4% paraformaldehyde in PBS. The brains, hearts, livers, and kidneys were dissected, postfixed in the same solution, cryoprotected with 30% sucrose in PBS for 48 h, and then frozen. Coronal sections (thickness of 40 μm) were cut on a microtome with a freezing unit, collected in PBS (pH 7.4), and divided into series. Tissue sections were incubated overnight with primary antibodies at 4°C. The primary antibodies used, their sources, and the dilutions used for immunohistochemistry were GFP (chicken, Abcam, 1:1,000–1:10,000; or rabbit, Abcam, 1:1000); tyrosine hydroxylase (TH) (mouse, Dia-Sorin, 1:800); AADC (rabbit, 1:5000; provided by Nagatsu I., Fujita Medical University); the neuronal marker NeuN (mouse, Millipore, 1:100); the astrocyte marker glial fibrillary acidic protein (GFAP) (rabbit, Covance, 1:1000); the Choline Acetyltransferase (ChAT) (mouse, CHEMICON, 1:200); and the Purkinje cell marker calbindin (mouse, SIGMA, 1:1000). The secondary antibodies used, their sources, and the dilutions used to detect the primary antibodies were Alexa Fluor 488 goat anti-chicken IgG (1:1000; Invitrogen); Alexa Fluor 594 goat anti-mouse IgG (1:1000; Invitrogen); Alexa Fluor 405 goat anti-mouse IgG (1 : 200; Invitrogen); and Alexa Fluor 594 goat anti-rabbit IgG (1:1000; Invitrogen). Immunofluorescent signals were assessed with a confocal laser scanning microscope (FV10i; Olympus, Tokyo).

2.4. Quantification of Gene Expression. The numbers of GFP/NeuN double-positive cells in the brain were counted using a stereological method. One in every five coronal sections covering either the frontal cortex, hippocampus, or amygdala of vector-injected mice was processed. Cell counting was performed in total on eight sections of each region of interest. Magnified images were taken using a 10 × objective lens (NA 0.5) at multiple different focal planes to visualize all cells in the thickness.

3. Results

3.1. Global Brain Transduction Was Achieved with Tyrosine-Mutant AAV9/3 Vectors. We generated pseudotype tyrosine-mutant AAV9/3 vectors, administered the vectors to adult mice with intracardiac injections, and then evaluated brain transduction. Mutant AAV9 capsid proteins containing two residues, where phenylalanine was substituted for tyrosine (Y446F and Y731F), encapsulated the vectors. The vectors were also engineered to express GFP under control of the CAG promoter (yfAAV9/3-CAG-GFP). Four weeks after administration (1.2×10^{11} vectors genome/mouse), widespread and extensive brain transductions were observed (Figures 1(a)–1(d)). Immunohistochemistry experiments demonstrated that most GFP-immunoreactive (GFP-IR) cells had glial cell morphologies and expressed the glial cell marker glial fibrillary acidic protein (GFAP) (Figure 1(f)). Robust GFP expression was observed in peripheral organs including the heart, liver, and kidney (Figures 1(g)–1(i)).